ENGI48415 Turbomachinery and Propulsion Coursework (Junya Ogawa)

Task A

From a performance study conducted on the GEnx-1B70 turbofan engine with bypass ratio $\beta = 9.1$ [1]:

η_{inlet}	η_{fan}	η_{LPC}	η_{HPC}	η_{CC}	η_{HPT}	η_{LPT}	η_{bypass}	η_{noz}
0.97	0.91	0.91	0.91	0.99	0.92	0.91	0.96	0.96

Table 1: Table of component efficiencies for GEnx-1B70 turbofan

Note: LPC stands for Low-Pressure Compressor, HPC for High Pressure Compressor, CC for Combustion Chamber, HPT for High Pressure Turbine and LPT for Low Pressure Turbine.

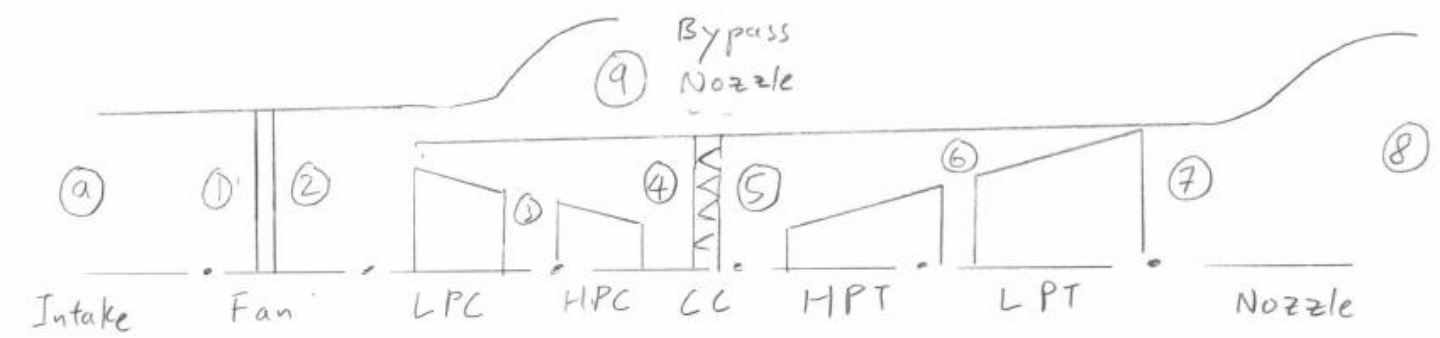

Figure 1: Schematic of GEnx-1B70 Turbofan with outlined stations a-9. Diagram not to scale.

Pressure ratios from [1]:

r_p^{fan}	r_p^{LPC}	r_p^{HPC}
1.5	1.3	22.3

Table 2: Table of pressure ratios of compressor components

From the design specifications (assuming a cruising altitude of $z = 11000m$) as well as Equation 1:

T_a (K)	T_{05} (K)	P_a (bar)	M_a	γ_a	γ_f	R_a $(J\ kg^{-1}K^{-1})$	R_f $(J\ kg^{-1}K^{-1})$	C_p^a $(J\ kg^{-1}K^{-1})$	C_p^f $(J\ kg^{-1}K^{-1})$
216.8	1470	0.227	0.78	1.4	1.33	287	273	1010	1100

Table 3: Table of thermodynamic data at cruising conditions

$$\gamma_f = \frac{C_p^f}{C_v^f} = \frac{C_p^f}{C_p^f - R_f} \Rightarrow R_f = C_p^f - \frac{C_p^f}{\gamma_f} = 272.932\ J\ kg^{-1}K^{-1} \quad (1)$$

From ambient to stagnation values (note all values of temperature and pressure will be given in terms of degree Kelvin and bars respectively unless otherwise specified):

$$T_{0a} = T_a\left(1 + \frac{\gamma_a + 1}{2}{M_a}^2\right) = 243.1802 \quad (2)$$

$$\frac{P_{0a}}{P_a} = \left(\frac{T_{0a}}{T_a}\right)^{\frac{\gamma_a}{\gamma_a - 1}} \Rightarrow P_{0a} = P_a\left(1 + \frac{\gamma_a + 1}{2}{M_a}^2\right)^{\frac{\gamma_a}{\gamma_a - 1}} = 0.3393 \quad (3)$$

Inlet calculations:

$$T_{01} = T_{0a} = 243.1802$$

$$\eta_{inlet} = \frac{T_{01s} - T_a}{T_{01} - T_a} \Rightarrow T_{01s} = T_a + \eta_{inlet}(T_{01} - T_a) = 242.3888 \quad (4)$$

$$\therefore \frac{P_{01s}}{P_a} = \left(\frac{T_{01s}}{T_a}\right)^{\frac{\gamma_a}{\gamma_a - 1}} \Rightarrow P_{01} = P_{01s} = P_a \left(\frac{T_{01s}}{T_a}\right)^{\frac{\gamma_a}{\gamma_a - 1}} = 0.3354 \tag{5}$$

Fan calculations:

$$P_{02} = P_{01} r_p^{fan} = 0.5032 \tag{6}$$

Rearranging Equation 5:

$$\frac{T_{02s}}{T_{01}} = \left(\frac{P_{02s}}{P_{01}}\right)^{\frac{\gamma_a - 1}{\gamma_a}} = \left(r_p^{fan}\right)^{\frac{\gamma_a - 1}{\gamma_a}} \Rightarrow T_{02s} = T_{01}\left(r_p^{fan}\right)^{\frac{\gamma_a - 1}{\gamma_a}} = 273.0486 \tag{7}$$

$$\eta_{fan} = \frac{T_{02s} - T_{01}}{T_{02} - T_{01}} \Rightarrow T_{02} = T_{01} + \frac{1}{\eta_{fan}}(T_{02s} - T_{01}) = 276.0027 \tag{8}$$

LPC calculations using Equations 6 – 8:

$$P_{03} = P_{02} r_p^{LPC} = 0.6541$$

$$T_{03s} = T_{02}\left(r_p^{LPC}\right)^{\frac{\gamma_a - 1}{\gamma_a}} = 297.4874$$

$$T_{03} = T_{02} + \frac{1}{\eta_{LPC}}(T_{03s} - T_{02}) = 299.6122$$

HPC calculations using Equations 6 – 8:

$$P_{04} = P_{03} r_p^{HPC} = 14.5865$$

$$T_{04s} = T_{03}\left(r_p^{HPC}\right)^{\frac{\gamma_a - 1}{\gamma_a}} = 727.4271$$

$$T_{04} = T_{03} + \frac{1}{\eta_{HPC}}(T_{04s} - T_{03}) = 769.7385$$

CC calculations using energy balance equation. Note Turbine Entry Temperature $T_{05} = 1470$ [1]:

$$\dot{m}_a C_p^a T_{04} + f \eta_{CC} \dot{m}_a Q_R = \dot{m}_a (1 + f) C_p^f T_{05}$$

$$f = \frac{C_p^f T_{05} - C_p^a T_{04}}{\eta_{CC} Q_R - C_p^f T_{05}} = 0.0207 \tag{9}$$

Due to the high-pressure spool connection, the HPT drives the HPC [1] and so work done by the HPT is transferred to the HPC:

$$W_x^{HPT} = W_x^{HPC}$$

$$\dot{m}_c C_p^f (1 + f)(T_{05} - T_{06}) = \dot{m}_c C_p^a (T_{04} - T_{03})$$

$$T_{06} = T_{05} - \frac{C_p^a (T_{04} - T_{03})}{C_p^f (1 + f)} = 1047.1$$

$$\eta_{HPT} = \frac{T_{05} - T_{06}}{T_{05} - T_{06s}} \Rightarrow T_{06s} = T_{05} - \frac{T_{05} - T_{06}}{\eta_{HPT}} = 1010.3261 \tag{10}$$

$$\frac{P_{06}}{P_{05}} = \left(\frac{T_{06s}}{T_{05}}\right)^{\frac{\gamma_f}{\gamma_f - 1}} \Rightarrow P_{06} = P_{05}\left(\frac{T_{06s}}{T_{05}}\right)^{\frac{\gamma_f}{\gamma_f - 1}} = 3.1859 \quad (11)$$

LPT calculations. As the low-pressure spool drives the LPC and the fan [1]:

$$W_x^{LPT} = W_x^{LPC} + W_x^{fan}$$

$$\dot{m}_a C_p^f (1+f)(T_{06} - T_{07}) = \dot{m}_a C_p^a (T_{03} - T_{02}) + \dot{m}_a C_p^a (1+\beta)(T_{02} - T_{01})$$

$$T_{07} = T_{06} - \frac{C_p^a\left((T_{03} - T_{02}) + (1+\beta)(T_{02} - T_{01})\right)}{C_p^c(1+f)} = 727.6612$$

Similar to the HPT, Equations 10 – 11 are used:

$$T_{07s} = T_{06} - \frac{T_{06} - T_{07}}{\eta_{LPT}} = 696.0684$$

$$P_{07} = P_{06}\left(\frac{T_{07s}}{T_{06}}\right)^{\frac{\gamma_f}{\gamma_f - 1}} = 0.6145$$

These calculations were then repeated using Equations 1 – 11 at maximum thrust (where $\dot{m}_a$ was known, $M_a = 0, z = 0, T_a = 288.15, P_a = 1.0133$) [1] to give an estimate of the exit main nozzle area A_8 and exit bypass nozzle area A_9 as it is assumed that $A_{8,9}$ are constant regardless of flight conditions:

	Cruising Conditions		Maximum Thrust Conditions	
Stations	$T_0\ (K)$	$P_0\ (bar)$	$T_0\ (K)$	$P_0\ (bar)$
a	243.1802	0.3393	288.1500	1.0133
1	243.1802	0.3354	288.1500	1.0133
2	276.0027	0.5032	327.0421	1.5200
9	276.0027	0.5032	327.0421	1.5200
3	299.6122	0.6541	355.0176	1.9759
4	769.7385	14.5865	912.0814	44.0634
5	1470.0000	14.4407	1690.0000	43.6227
6	1047.1025	3.1859	1190.1543	9.1379
7	727.6612	0.6145	805.6096	1.5601
8	727.6612	0.6145	805.6096	1.5601

Table 4: Stagnated temperature and pressure values at Stations a-7 in both cruise and maximum thrust conditions

Note that for our calculations, the bleed station from the LPC [1] has been left out (unlike in the real GEnx-1B70 Turbofan) for simplified calculations.

For maximum thrust conditions, at the exit of the main nozzle 08:

$$\because P_{07} > P_a, \therefore P_{08} = P_{07}, M_8 = 1$$

$$T_8 = \frac{T_{08}}{\left(1 + \frac{\gamma_f + 1}{2} {M_8}^2\right)} = \frac{2T_{08}}{\gamma_f + 1} = 691.5104 \quad (12)$$

$$\eta_{noz} = \frac{T_{07} - T_8}{T_{07} - T_{8s}} \Rightarrow T_{8s} = T_{07} - \frac{T_{07} - T_8}{\eta_{noz}} = 686.7562 \quad (13)$$

$$u_8 = \sqrt{2C_p^c(T_{08} - T_8)} = 501.0172 \quad (14)$$

$$P_8 = P_{08}\left(\frac{T_{8s}}{T_{08}}\right)^{\frac{\gamma_f}{\gamma_f - 1}} = 0.8199$$

Given $\dot{m}_a = 114.3990\ kgs^{-1}$ at maximum thrust [1]:

$$\rho_8 = \frac{P_8}{R_f T_8} = \frac{\dot{m}_a}{A_8 u_8} \tag{14}$$

$$A_8 = \frac{\dot{m}_a R_f T_8}{P_8 \times 10^5 \times u_8} = 0.5472\ m^2 \tag{15}$$

Similarly, for the exit of the bypass nozzle 09 Equations 12 – 15 are used but using γ_a instead:

$$\because P_{02} > P_a, \therefore P_{09} = P_{02}, M_9 = 1$$

$$T_9 = \frac{2T_{09}}{\gamma_a + 1} = 272.5351$$

$$T_{09} = T_{02} - \frac{T_{02} - T_9}{\eta_{bypass}} = 270.2640$$

$$u_9 = \sqrt{2C_p^a(T_{09} - T_9)} = 331.8195$$

$$P_9 = P_{09}\left(\frac{T_{9s}}{T_{09}}\right)^{\frac{\gamma_a}{\gamma_a - 1}} = 0.7798$$

Given $\dot{m}_\beta = 1041.3\ kgs^{-1}$ at maximum thrust [1]:

$$A_9 = \frac{\dot{m}_\beta R_a T_9}{P_9 \times 10^5 \times u_9} = 2.9646\ m^2$$

Using both values of $A_{8,9}$ into the main calculations at cruising altitude:

$$T_{08} = T_{07}, P_{08} = P_{07}$$

Since $P_{08} = P_{07} < P_a$, flow is choked. Using Equations 12 – 14:

$$M_8 = 1$$

$$\therefore T_8 = \frac{2T_{08}}{\gamma_f + 1} = 624.6019$$

$$T_{8s} = T_{07} - \frac{T_{07} - T_8}{\eta_{noz}} = 620.3077$$

$$u_8 = \sqrt{2C_p^c(T_{08} - T_8)} = 476.1622\ ms^{-1}$$

$$P_8 = P_{08}\left(\frac{T_{8s}}{T_{08}}\right)^{\frac{\gamma_f}{\gamma_f - 1}} = 0.3229$$

$$\therefore \dot{m}_c = \rho_8 A_8 u_8 = \frac{P_8 \times 1 \times 10^5 \times A_8 u_8}{R_f T_8} = 47.4087\ kgs^{-1} \tag{16}$$

Bypass nozzle calculations using Equations 12-14 and 16:

$$T_{09} = T_{02}, P_{09} = P_{02}$$

Note $P_{09} = P_{02} > P_a$ so flow is choked:

$$M_9 = 1$$

$$T_9 = \frac{2T_{09}}{\gamma_a + 1} = 230.0022$$

$$T_{9s} = T_{02} - \frac{T_{02} - T_9}{\eta_{bypass}} = 228.0855$$

$$u_9 = \sqrt{2C_p^a(T_{09} - T_9)} = 304.0517\ ms^{-1}$$

$$P_9 = P_{09}\left(\frac{T_{9s}}{T_{09}}\right)^{\frac{\gamma_a}{\gamma_a - 1}} = 0.5032$$

All values of T_{08}, P_{08}, T_{09} and P_{08} were then inputted back into Table 4. To calculate the various mass flow rates at cruising condition (all are in units of $kg\ s^{-1}$):

$$\dot{m}_a = \frac{\dot{m}_c}{1 + f} = 46.4462 \tag{17}$$

$$\dot{m}_f = f\dot{m}_a = 0.9625 \tag{18}$$

$$\dot{m}_\beta = \beta\dot{m}_a = 422.6605 \tag{19}$$

Therefore, at cruising condition:

$$u = M_a a = 0.78 \times 295.2 = 230.2560\ ms^{-1} \tag{20}$$

$$F_T = \dot{m}_c\big((1 + f)u_8 - u\big) + A_8(P_8 - P_a) \times 10^5 + \dot{m}_\beta(u_9 - u) + A_9(P_9 - P_a) \times 10^5 = 58.0242\ kN \tag{21}$$

Thus, the Thrust-Specific Fuel Consumption (TSFC) is given by:

$$TSFC = \frac{\dot{m}_f}{F_T} = 0.0166\ kg\ s^{-1}kN^{-1} \tag{21}$$

Note the initial given TSFC $TSFC_0$:

$$TSFC_0 = 0.5\ kg\ h^{-1}\ kg^{-1} = 0.5 \times \frac{1\ h^{-1}}{60^2\ s^{-1}} \times \frac{1000\ kN^{-1}}{9.81\ N^{-1}} = 0.0142\ kg\ s^{-1}kN^{-1}$$

$$\%\ difference = \left(\frac{TSFC - TSFC_0}{TSFC_0}\right) \times 100\% = 16.90\%$$

Which means that the calculated TSFC value is around 16.9% higher than the given TSFC value which makes this choice of high-bypass turbofan ideal for our simulations due to its high accuracy.

At stable cruising condition the lift force is equal to the aeroplane weight and the thrust equal to the aeroplane drag so, an equation for the required thrust F_{T0} can be calculated using the lift-drag ratio $\frac{L}{D}$ and weight W:

$$\frac{L}{D} = \frac{W}{F_{T0}} = 21.6 \tag{22}$$

The weight was calculated using the maximum payload as a worst-case scenario (i.e., with full fuel and passenger capacity):

$$\frac{W}{F_{T0}} = \frac{mg}{F_{T0}} = \frac{9.81 \times 176000}{F_{T0}} \Rightarrow F_{T0} = \frac{9.81 \times 176000}{21.6} \approx 79.9333\ kN \tag{23}$$

As the aeroplane runs on two engines the total thrust produced at cruise would be $2 \times 58.0242 = 116.0484\ kN$ which exceeds F_{T0} so the engine meets the minimum requirements. However, in the case of single engine failure it is imperative that the aeroplane loses altitude and speed to increase the maximum thrust of the engine (as this increases ambient temperature and pressure as well as mass flow rates) albeit with reduced range as $F_T < F_{T0}$ for operation. It should also be noted that in take-off a portion of the fuel mass will be burnt-off so this would also likely reduce F_{T0} as well.

In addition, using the Boeing 787-8 as an example of an aeroplane which uses the GEnx-1B70, the maximum time t_{max} the 787-8 can fly was obtained. Note the total fuel mass m_f (obtained from [2]) is divided by 2 due to the 787-8 being a 2-engine aeroplane:

$$m_f = 101343\ kg$$

$$t_{max} \approx \frac{m_f}{2\dot{m}_f} \times \frac{1\ h}{60^2 s} = \frac{101343}{0.9625} \times \frac{1}{3600} = 14.62\ h \tag{24}$$

From specifications, Equation 24 and F_{T0}, the maximum time using specifications t_{max0} is calculated:

$$m_{f0} = 27800\ kg, \dot{m}_{f0} = TSFC_0 \times F_{T0} = 0.0141578 \times 79.9333 = 1.1317 kg\ s^{-1}$$

$$t_{max0} \approx \frac{m_{f0}}{2\dot{m}_{f0}} \times \frac{1\ hr}{60^2 s} = \frac{27800}{1.1317} \times \frac{1}{3600} = 6.82\ h$$

Thus, the engine used in calculations lasts longer in the air (14.62 hours compared to 6.82 hours requirement) at the same cruising speed, which makes this choice of high bypass turbofan ideal. However, it is noted that the specification has a reduced range and speed compared to other aircraft.

Task B

Initial values were calculated from Task A as well as [2] (for N_{stages}) and [3] (ω) for initial input into MEANGEN.X to obtain a prototype HPT design:

Initial Values	$\dot{m}_c$ $(kg\ s^{-1})$	R	ψ	ϕ	T_{in} (K)	P_{in} (bar)
	47.4087	0.5838	0.8325	0.6000	1470	14.4407
η_{stage}	Flow Type	ω (rpm)	r_{tip} (m)	R_f $(Jkg^{-1}K^{-1})$	γ_f	N_{stages}
0.92	Axial	11377	0.4437	272.932	1.33	2

Table 5: Input inlet values into MEANGEN for Run 1. Values taken from Task A, [2] and [3]

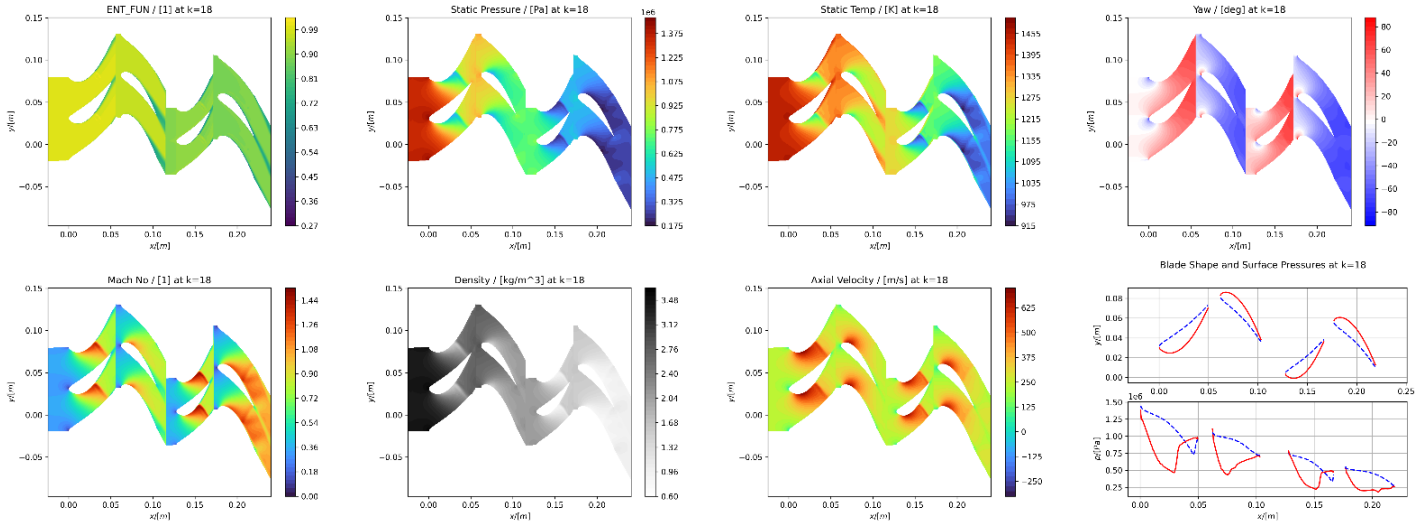

Figure 2: Thermodynamic variable plots for k = 18 for Run 1

Run 1 was run on MULTALLOPEN using values from **Table 5**, which yielded a turbine with $\eta_{tt} = 91.308\%$. Major sources of η_{tt} loss is due to a few reasons: Firstly, shock formations in stators (and 2nd rotors to certain extent), as seen in the Mach No Plot. In **Figure 2**, due to shocks, entropy is generated via shock formula $\Delta S \propto (M^2 - 1)^3$ where M is Mach number perpendicular to shockwave. Secondly, flow separation at trailing edges leads to high amounts of entropy formation where eddies form (as shown the ENT_FUN plot). As $T\dot{S} = \dot{m}_c({V_m}^2 - V_m V_c \cos\alpha)$, for $\dot{S}$ to reduce α needs to be reduced and thus trailing edge needs to be thinner. Therefore, the best way to increase η_{tt} and reduce entropy is to make intra-blade area smaller by reducing thickness, which should let flow expand fully.

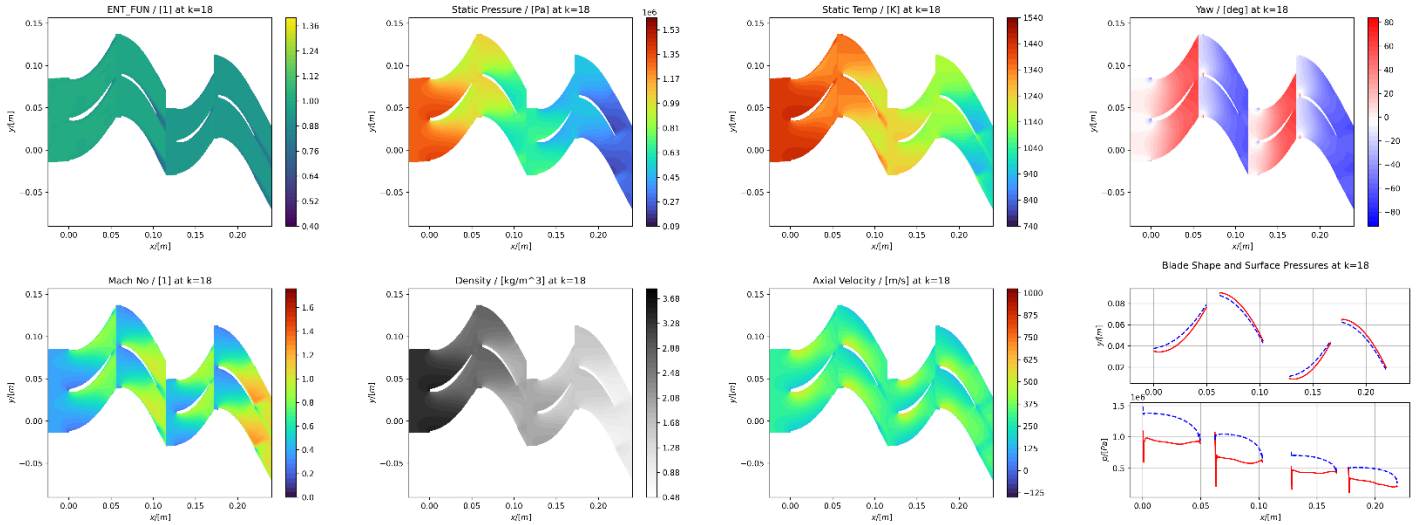

Figure 3: Thermodynamic variable plots for k = 18 for Run 2

After some experimentation, the relative thickness of the stator and rotor blades were reduced to 10% and 7% respectively in Run 2 via editing the meangen.dat file blade thicknesses. This gave an optimal $\eta_{tt} = 94.212\%$, which was an improvement of around 3.180%. However, there are what appears to be some major shocks occurring around the 2nd rotor exit as well as well as some accelerated flow in the 1st rotor exit in **Figure 3**, so more 2D design techniques applications are needed to further optimise the 2D profile.

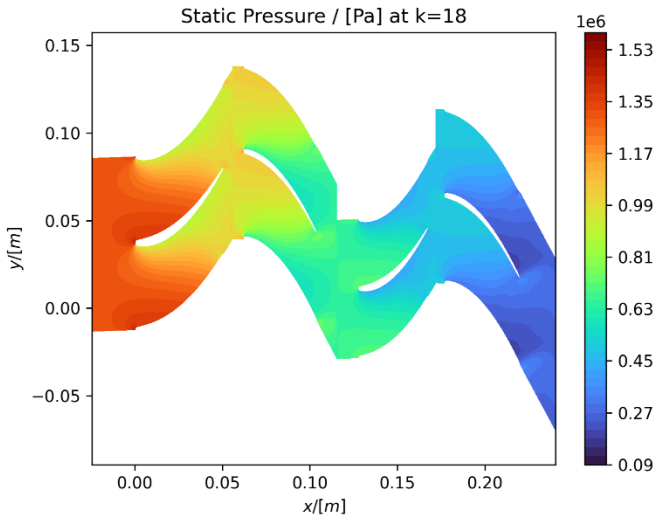

Figure 5: Static Pressure plot at k = 18 at Run 3

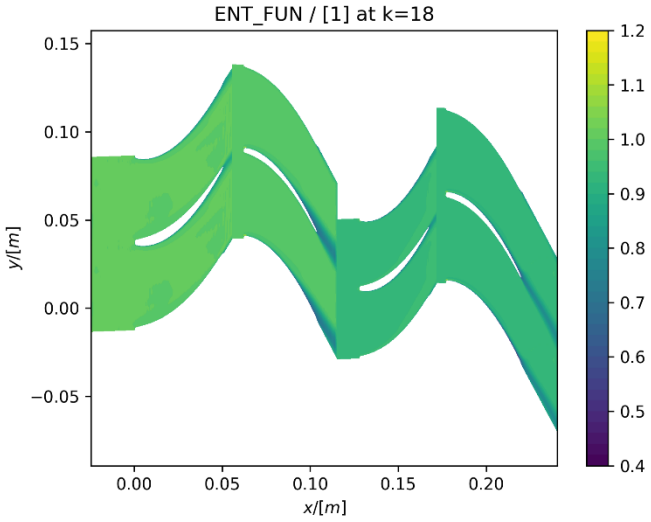

Figure 4: ENT_FUN plot at k = 18 at Run 3

Run 3 occurred with a shifting of blade centres towards leading edges in Run 3 to relative centres of 40% and 35% respectively within meagnen.in. This caused η_{tt} to increase to 94.235%, a further improvement of 0.0244%. Flow seemed to be much better with shocks eliminated in all stators (blade rows 1-3) but still present in 2nd rotor exit (blade row 4) as can be seen in **Figure 4**. Furthermore, it was also found that this was the optimum 2D set-up, as lowering blade count in 2nd rotor or reducing thickness to reduce intra-blade area to avoid shocks caused η_{tt} to decrease. As seen in **Figure 5** there is still some flow separation present but as mentioned earlier, any attempt to reduce α led to a decrease in η_{tt} so the flow separation was tolerated. Thus, the 2D blade profile shape was deemed to have been sufficiently optimised, as there were no other foreseeable 2D optimisations to carry out. 3D techniques will now be used to further improve η_{tt}.

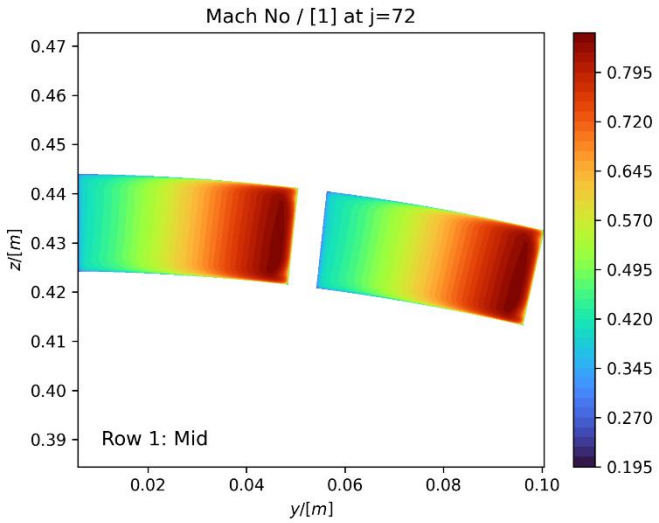

Figure 6: Mach No plot at middle of 1st stator before stator compound lean (Run 3)

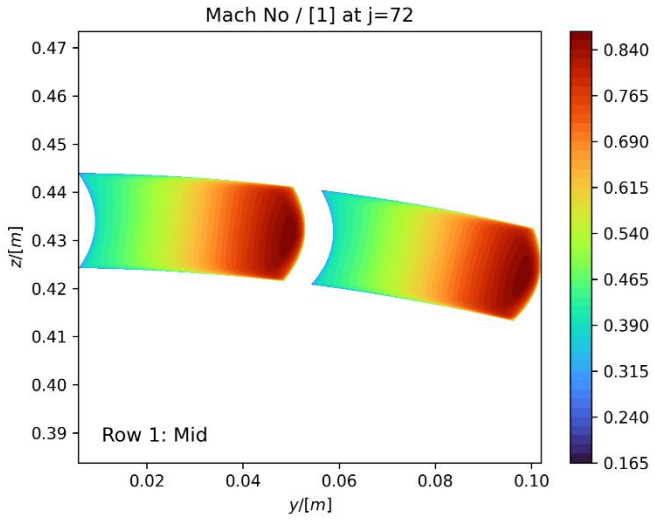

Figure 7: Mach No plot at middle of 1st stator after 7% stator compound lean (Run 5)

Run 4 implemented a compound lean on the stator blades (Blade Rows 1 and 3) of around 5% in stagen.dat. This was done by editing FLEAN of Section 2 in Blade Rows 1 and 3 within Card 27 of stagen.dat to 0.05, which made the suction surface of the stator blades extrude towards the pressure surface. This resulted in η_{tt} having increased to 94.339%, an increase of 0.11%. As can be seen in **Figures 6 and 7**, compound lean caused the flow to be directed towards the midspan of the blade stack, which allows more work to be done there, as the range of Mach numbers increased with compound lean (from the contour legend) especially at midspan. Thus, the work done is more efficient and improves η_{tt} as entropy generated is also reduced.

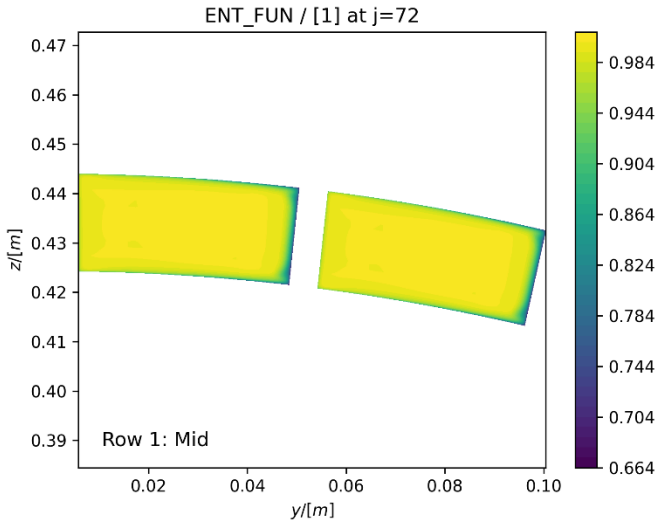

Figure 8: ENT_FUN at middle of 1st stator before stator compound lean (Run 3)

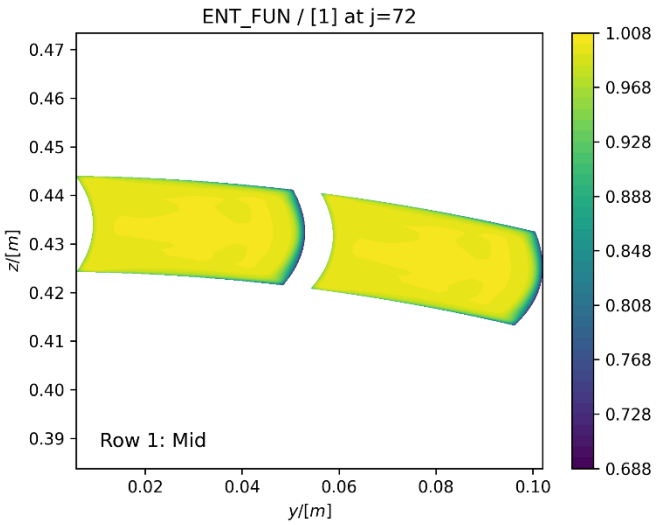

Figure 9: ENT_FUN at middle of 1st stator after 7% stator compound lean (Run 5)

This is also seen in the general increase of the ENT_FUN range in the contours in **Figures 8 and 9**, which meant the average entropy generated decreased upon compound lean implementation. Run 5 further optimised the stator lean value to 7% as it was felt like the FLEAN value could be improved upon. This resulted in $\eta_{tt} = 94.344\%$, a relative increase of 0.005%. Further increases to the FLEAN value only served to decrease η_{tt} so FLEAN in the stators was deemed sufficiently optimised.

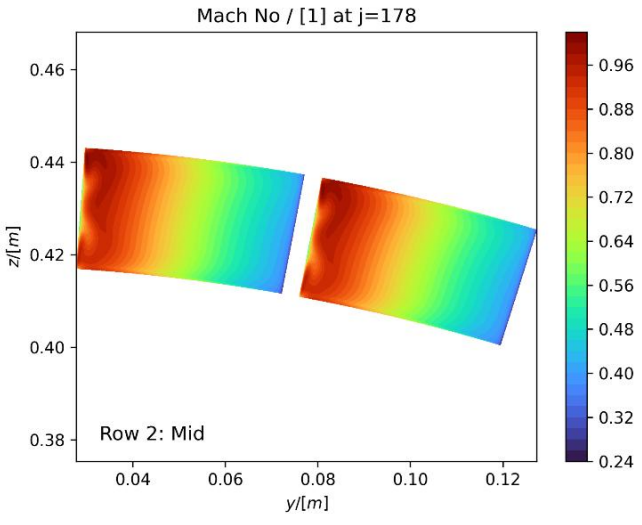

Figure 10: Mach no plot in middle of 1st rotor before rotor compound lean (Run 5)

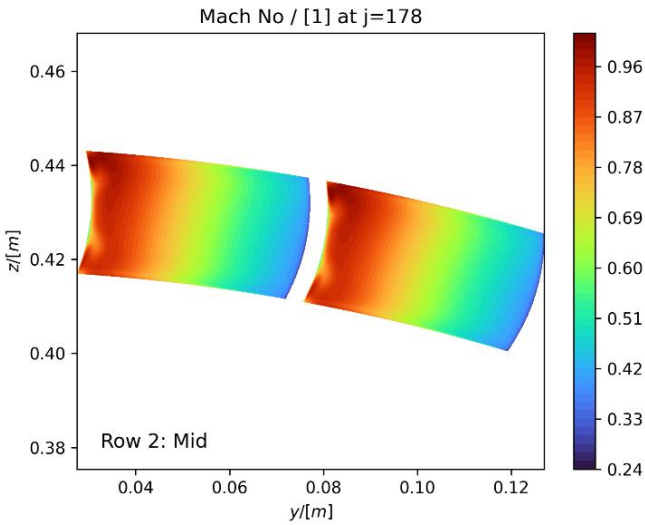

Figure 11: Mach no plot in middle of 1st rotor after 5% rotor compound lean (Run 6)

Run 6 aimed at trying to improve the 3D blade stacking of the rotors via implementing compound lean. This was because secondary flows arising from boundary layer conditions were noticed in **Figure 10**. These secondary flows

will generate entropy due to viscous stresses interaction with the primary flow. Therefore, a 5% FLEAN was set for section 2 of blade stacks 2 and 4 at Card 27. This resulted in η_{tt} increasing to 94.385%, a 0.044% increase.

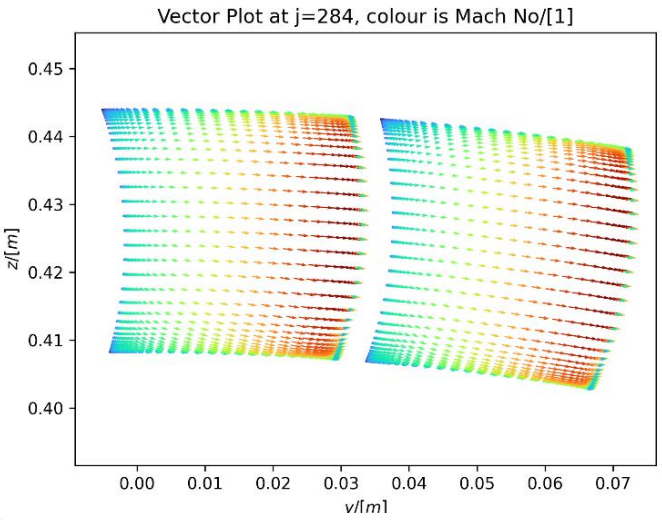

Figure 12: Mach Vector plot at 2nd stator before hub clearance (Run 6)

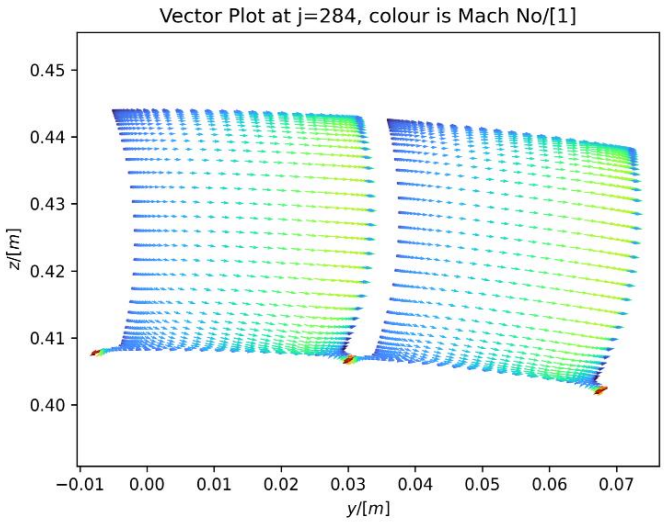

Figure 13: Mach Vector plot at 2nd stator after hub clearance (Run 7)

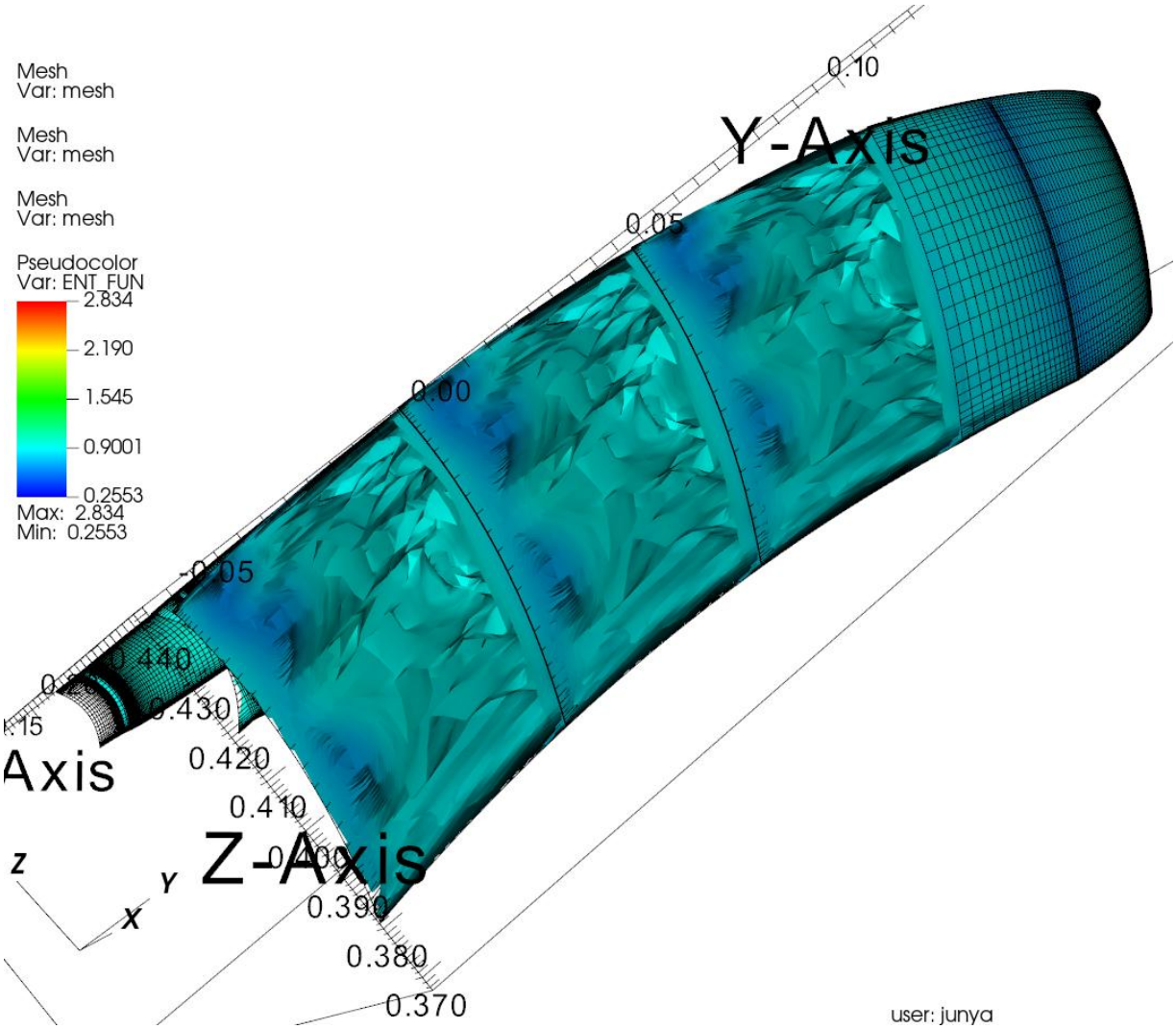

Figure 14: Iso-surface plot of ENT_FUN for Run 7 using log scale,

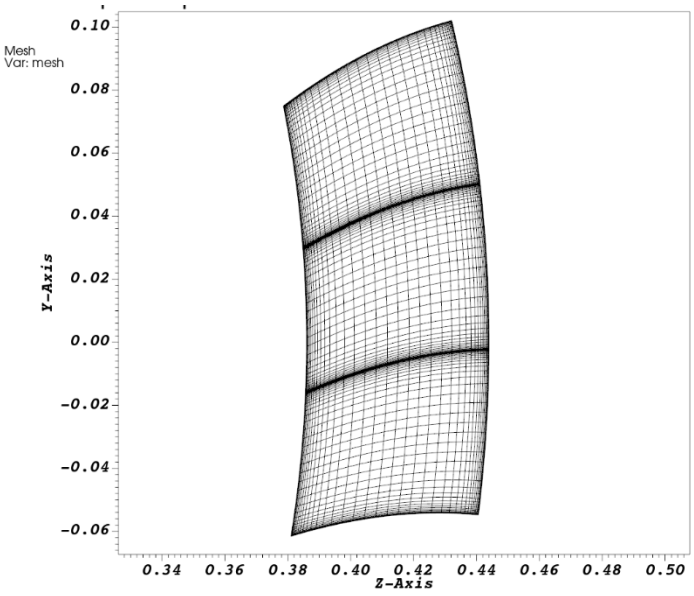

Figure 15: Mesh at j = 433 before refinement (Run 7)

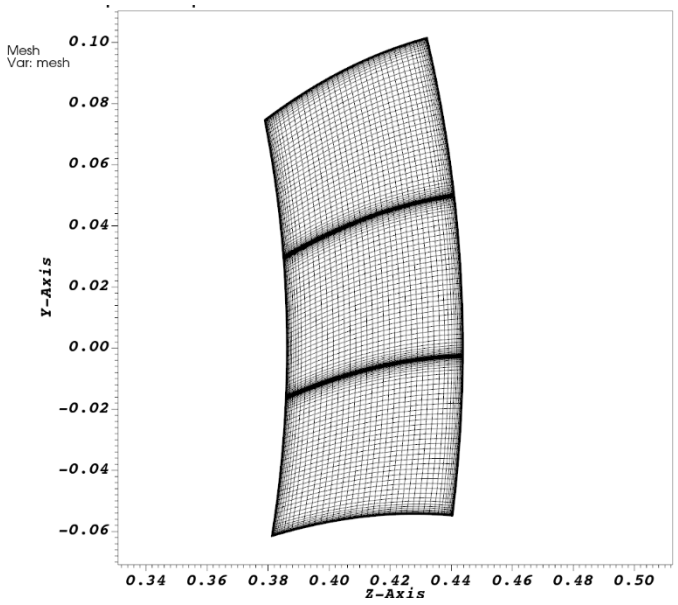

Figure 16: Mesh at j = 433 after refinement (Run 8)

Run 7 implemented hub and tip clearances to simulate realistic gap losses. This was done via editing the KTIPS, KTIPE and FRACTIP values of Card 13 of stagen.dat: hub clearances for stators were defined as having a FRACTIP value of 0.5% from KTIPS of 1 to KTIPS of 4, whilst for rotors tip clearances were defined as having the same FRACTIP value of 0.5% but now with KTIPS value of 34 to KTIPE value of 37. It was found that η_{tt} decreased to 93.111%, a 1.349% decrease compared to Run 6. This is due to the hub clearance (in this example) causing a primary flow of the pressure gradient from the suction to pressure surface (clockwise) meeting a secondary flow which originated from the pressure surface going into the pressure surface (counterclockwise) which generated an overall velocity vector in the counterclockwise in **Figure 13**. As mentioned previously, the mixing of fluids generates entropy, which can also be seen in **Figure 14**, where there is now a smaller secondary flow vortex (with low ENT_FUN) at the tip surface in comparison to the larger secondary flow vortexes near the midspan which were generated from the flow separation at the trailing edge.

To ensure accuracy, the 8th and final run increased the mesh quality by increasing the IM and KM count in Card 2 of stagen.dat such that the cell count increased by 100%, from a value of $37^2 \times 434 = 594146$ cells to a new cell count of 1188292, which meant IM and KM were changed from 37 to 52, as visualised in **Figures 15 and 16** within Card 2 in stagen.dat. This also meant having to change the KTIPS and KTIPE values for hub and tip clearances such that they were in proportion to the k cell count: for tip clearances this was changed to 47 – 52, whilst for hub clearances this was 1 – 6. η_{tt} had decreased to a final value of 92.938%, a 0.186% decrease. Outputs from the MULTALLOPEN programme revealed that this machine had an overall power output of 20508kW. As the theoretical power output is given by $W_x = C_p^f(T_{05} - T_{06})\dot{m}_c = 22053\ kW$, which had a mechanical efficiency $\eta_{mech} \approx 92.99\%$. Furthermore, a table of η_{tt} and relative % increase was compiled according to run number as shown below:

Run No.	1	2	3	4	5	6	7	8
η_{tt} (%)	91.308	94.212	94.235	94.339	94.344	94.385	93.111	92.938
% increase	N.A.	3.169	0.024	0.110	0.005	0.044	−1.350	−0.186

Table 6: Table of total-to-total efficiencies as well as % increases across 7 runs

This showed that in respect to Run 1, Run 8 had an increase of 1.79% in η_{tt} with 2D profiling optimisation, 3D stator and rotor compound lean, tip and hub clearances as well as mesh refinement. The biggest relative % increase occurred between Runs 1 and 2, where the 2D blade relative thickness was reduced to 10% and 7%. The smallest relative % increase was between runs 4 and 5, where the stator compound lean increased from 5% to 7%.

Task C

To talk about the contribution of a cycle design choice on its sustainability, a good way would be to discuss the Thrust-Specific Fuel Consumption (TSFC) because of design choices, as it determines how much fuel an aircraft consumes per unit thrust. The cycle discusses in Task A has a cruising TSFC of 16.5884 $g\ s^{-1}\ kN^{-1}$ (which is based on the GEnx-1B70 engine from 2006), which is slightly higher compared to its counterparts. Looking at more modern counterparts, the Rolls-Royce Trent 7000 series released in 2015 has a cruising TSFC of 14.3 $g\ s^{-1}\ kN^{-1}$ [4], which is around a 13.8% decrease to the Task A design. This meant per unit thrust, the Trent 7000 consumed about 13.8% less fuel which means the Task A design cycle is not as sustainable compared to its modern counterparts. Furthermore, there is research being done about replacing the current kerosene fuel used in turbojets to hydrogen. This is slated to have compounded improvements of up to a 10% decrease in TSFC [5] to its kerosene counterparts, which is also in part due to the higher Lower Heating Value (LHV) of hydrogen [5]: hydrogen has a LHV of 120MJ/kg compared to kerosene's 43MJ/kg, a 179% increase in fuel density. This makes our turbojet's TSFC not very sustainable compared to newer turbojet designs. However, there are a few methods of increasing the TSFC. One of them is to increase the main nozzle area, which would increase thrust and thus decrease TSFC. Another method would be to optimise the aerodynamics of the plane to reduce drag as much as possible, which would then naturally improve thrust and thus reduce TSFC. All these methods could be considered into future studies into similar propulsion cycles.

However, the turbine design process tells a different story. A study which implemented positive compound lean on stator blades had increase of η from 95.69 to 95.71 [6], an increase of 0.021% which was smaller than results seen in Task B's 4th to 6th runs, where because of compound lean η increased by 0.158% from 94.235% to 94.384%. This shows the 3D design methods used in this paper yielded better η improvements than some literature studies. Furthermore, reducing the blade's relative thickness allowed for less material to be used during manufacture whilst simultaneously increasing η via reducing entropy generation. However, if the blades are too thin, the loading caused by the viscous stresses in the flow will cause component failure. This component failure will require more material to repair which will adversely affect performance and sustainability goals. Therefore, there needs to be balance between an efficient engine as well as the stress requirements of the blades. In addition, improved compound lean means less wear and tear on the turbine so less need for maintenance. This is because more efficient work done means that the turbine components would not wear down so easily, which makes the aircraft more efficient as it can spend more time in the sky. In general, improving η of the HPT means that more useful energy is generated to supply the compressor and there will lesser losses to entropy formation, as well as saving on important criteria such as payload or maintenance period. From the conclusions made in Task B, priority should be given to 2D blade profiling optimisation, as it has the most potential at improving efficiency.

Lastly, the design work here collaborates with the UN's Sustainable Developmental Goals (SDG), or more specifically, SDG No. 12 – Sustainable Production and Consumption [7]. In the context of a turbofan, this means the consumption of fuel should be as low as possible so less greenhouse gases are emitted from the combustion of kerosene. A lesser demand for kerosene also means less production which also reduced greenhouse gases emissions. Furthermore, aircraft have been known to be heavy polluters. Taking the United States as an example, aircraft constitute around 10% of transport emissions [8] and around 3% of the national greenhouse gas emissions [8]. Thus, there is a need for the aircraft manufacturing industry to make their engines as efficient as possible to limit CO2 emissions. Given this, actions must be made to reduce greenhouse gases emissions of aircraft. For example, Rolls Royce is conducting research into constructing an ultra-high bypass engine, which will reduce NOx emissions by 25% [9]. The design choices made here in Task A and B can be applied to most turbomachinery, no matter the type of engine to determine how to best obtain the best TSFC as well as engine performance and efficiency.

Bibliography

[1] A. El-Sayed, M. S. Emeara, and M. A. El, "Performance Analysis of High Bypass Ratio Turbofan Aeroengine," *International Journal of Development Research*, vol. 6, no. 07, pp. 8382–8398, Jul. 2016, Accessed: Jan. 15, 2025. [Online]. Available: https://www.researchgate.net/publication/306082636_Performance_Analysis_of_High_Bypass_Ratio_Turbofan_Aeroengine

[2] Boeing Commercial Airplanes, "787 Airplane Characteristics for Airport Planning," Boeing, Crystal City, VA, 2023. Accessed: Jan. 21, 2025. [Online]. Available: https://www.boeing.com/content/dam/boeing/boeingdotcom/commercial/airports/acaps/787.pdf

[3] U.S. Department of Transportation, "Type Certificate Data Sheet E00078NE," Federal Aviation Administration, Apr. 2011. Accessed: Jan. 21, 2025. [Online]. Available: http://large.stanford.edu/courses/2016/ph240/ginsberg2/docs/E00078NERev3.pdf

[4] E. J. Adler and J. R. R. A. Martins, "Hydrogen-powered aircraft: Fundamental concepts, key technologies, and environmental impacts," *Progress in Aerospace Sciences*, vol. 141, no. 141, p. 100922, Aug. 2023, doi: https://doi.org/10.1016/j.paerosci.2023.100922.

[5] Rolls Royce Ltd., "Trent 7000," *Archive.org*, 2015. https://web.archive.org/web/20170222024549/http://www.rolls-royce.com/products-and-services/civil-aerospace/products/civil-large-engines/trent-7000.aspx (accessed Jan. 21, 2025).

[6] S. Zhang, D. G. MacManus, and J. Luo, "Parametric study of turbine NGV blade lean and vortex design," *Chinese Journal of Aeronautics*, vol. 29, no. 1, pp. 104–116, Feb. 2016, doi: https://doi.org/10.1016/j.cja.2015.12.005.

[7] United Nations, "The 17 sustainable development goals," *United Nations*, 2024. https://sdgs.un.org/goals

[8] J. Overton, "The Growth in Greenhouse Gas Emissions from Commercial Aviation," *www.eesi.org*, Jun. 09, 2022. https://www.eesi.org/papers/view/fact-sheet-the-growth-in-greenhouse-gas-emissions-from-commercial-aviation

[9] Rolls Royce Ltd., "UltraFan® The Ultimate TurboFan," 2022. Available: https://www.rolls-royce.com/~/media/Files/R/Rolls-Royce/documents/innovation/ultrafan-fact-sheet.pdf